UPWIND SUMMATION BY PARTS FINITE DIFFERENCE METHODS FOR LARGE SCALE ELASTIC WAVE SIMULATIONS IN COMPLEX GEOMETRIES [*]

KENNETH DURU[†], FREDERICK FUNG[‡], AND CHRISTOPHER WILLIAMS [§]

Abstract. High-order accurate summation-by-parts (SBP) finite difference (FD) methods constitute efficient numerical methods for simulating large-scale hyperbolic wave propagation problems. Traditional SBP FD operators that approximate first-order spatial derivatives with central-difference stencils often have spurious unresolved wave-modes in their numerical solutions. On marginally resolved computational grids, these spurious wave-modes have the potential to destroy the accuracy of numerical solutions for a first-order hyperbolic partial differential equation, such as the elastic wave equation. To ensure the accuracy of numerical solutions of the three space dimensional (3D) elastic wave equation in complex geometries, we discretise the 3D elastic wave equation with a pair of non-central (upwind) finite-difference stencils, on boundary-conforming curvilinear meshes. Using the energy method we prove that the numerical method is stable, and energy conserving. Furthermore, computational results show the robustness of the scheme. We present numerical simulations of the 3D elastic wave equation in heterogeneous media with complex non-planar free surface topography, including numerical simulations of community developed seismological benchmark problems. Our results show that the upwind SBP operators are more robust and less prone to numerical dispersion errors on marginally resolved meshes when compared to traditional SBP operators, thereby increasing efficiency.

Key words. Finite difference method, high-order accuracy, stability, boundary treatment, wave propagation

AMS subject classifications. 86A15, 65M06, 35-04

1. Introduction. High fidelity numerical simulations of seismic (elastic) waves are important in many applications such as earthquake engineering, natural minerals and energy resources exploration, as well in strong-ground motion analysis and underground fluid injection monitoring. Seismic waves emanating from geophysical events can propagate over hundreds to thousands of kilometres interacting with geological structure and complicated free-surface topography. Exploration seismology and natural earthquake hazard mitigation increasingly rely on multi-scale and high frequency (0–20 Hz) simulations. Surface and interface waves [16] are often the largest amplitude waves modes, and probably the most important wave modes in the medium. Therefore, accurate and efficient numerical simulation of seismic surface and interface waves, and scattering of high-frequency wave modes by complex non-planar free-surface topography are critical for assessing and quantifying seismic risks and hazards [8].

In this study, we derive high order accurate and efficient numerical methods for large scale numerical simulations of seismic waves in complex geometries. We consider the elastic wave equation in first order form, where the unknowns are the particle velocity and stress fields. The main classes of numerical methods for the solution of time-dependent PDEs are spectral method, finite element (FE) method, finite difference (FD) method, finite volume (FV) method and the discontinuous Galerkin (DG) finite element method. They all have different strengths and weaknesses. Computational efficiency has continued to make the use of FD methods on structured grids attractive. However, the presence of boundary conditions and complex non-planar free-surface topography make the design of stable and accurate FD methods challenging. For computational seismology, staggered grids FD methods on Cartesian meshes are the industry standard because they are efficient and have optimal numerical dispersion properties. However, the design of high order accurate and stable staggered FD methods for the elastic wave equation in complex geometries is a challenge. Although some progress is being made in this direction [15].

For well-posed initial boundary value problems (IBVP), the summation-by-parts (SBP) FD [18] with the simultaneous approximation term (SAT) [13, 11, 14] technique for implementing boundary conditions enables the development of stable numerical approximations on smooth geometries. The

methods can be extended to complex geometries using curvilinear coordinate transforms and multi-block schemes [4, 19]. Traditional SBP FD operator are based on central finite difference formula with special one-sided boundary closures, designed such that the operator preserves the integration by parts principle [18]. Often, traditional SBP FD operators which approximate the spatial derivative suffer from spurious unresolved wave-modes in their numerical solutions. For marginally resolved solutions, these spurious wave-modes have the potential to destroy the accuracy of numerical solutions for a first-order hyperbolic partial differential equation, such as the elastic wave equation.

To ensure the accuracy of numerical solutions of elastic wave equations in complex geometries, we discretise the 3D elastic wave equation with a pair of non-central (upwind) FD stencils [12], on boundary-conforming curvilinear meshes. The main benefit for these operators [12, 3] is that they can suppress poisonous spurious oscillations from unresolved wave-modes, which can destroy the accuracy of numerical simulations. However, these operators are asymmetric and dissipative, can potentially destroy symmetries that exist in the continuum problem. For example, the linear elastic wave equation with free-surface boundary conditions preserves the mechanical energy for all time. It is imperative that a stable numerical approximation must preserve these symmetries, by mimicking the corresponding continuous energy estimate at the discrete level. Otherwise numerical simulations on marginally resolved meshes can be polluted by numerical artefacts, in particular for longtime simulations. A good case in point is that important information in the medium propagated by scattered high frequency surface waves could be corrupted through numerical dissipation.

Our overall goal is to carefully combine the upwind SBP operator pair so that we preserve the discrete anti-symmetric property and invariants of the underlying IBVP. We then achieve energy stability by imposing boundary conditions weakly with penalty terms, in a manner that leads to bounded discrete energy estimates. In particular, if the IBVP is energy conserving, the numerical numerical approximation is also energy conserving. Numerical solutions are integrated in time using the fourth-order accurate low-storage Runge-Kutta method. The numerical method is implemented in WaveQLab [4] , a petascale elastic wave solver. Simulations of elastic waves in heterogeneous media with free surface topography are presented, including the numerical simulation of community developed seismological benchmark problems. Our results show that the upwind SBP FD operators are more robust and less prone to numerical dispersion on marginally resolved meshes when compared to traditional SBP operators [18, 4].

The structure of the paper is as follows. In the next section, we present the elastic wave equation in general curvilinear coordinates and prove anti-symmetric properties that must be preserved. In section 3, we introduce general linear well-posed boundary conditions and derive continuous energy estimates. In section 4, we discretise in space, introduce upwind SBP operators, and approximate the elastic wave equation in space. Numerical boundary conditions are derived in section 5 as well as the derivation of semi-discrete energy estimates, proving stability. In section 6, we present numerical simulations verifying the accuracy and demonstrating the efficacy of the numerical method in a complex geometry, with geologically constrained non-planar free-surface topography. In section 7, we draw conclusions and speculate on the directions for future work.

2. Preliminary. In this section we introduce the elastic wave equation in general curvilinear coordinates and derive invariants and anti-symmetric properties that must be preserved.

2.1. Physical model. Let Ω be a connected compact subset of $\mathbb{R}^3$ with a piecewise-smooth boundary Γ, $t > 0$ be the time variable, $\boldsymbol{\sigma} := (\sigma_{xx}, \sigma_{yy}, \sigma_{zz}\sigma_{xy}, \sigma_{xz}, \sigma_{yz})^T$ be the vector of stresses, and $\mathbf{v} := (v_x, v_y, v_z)^T$ be the particle velocities. Throughout, we assume that the velocities and stresses are bounded functions of space and time. The first order time-dependent elastic wave

equations in a source free, heterogeneous medium are

$$
(2.1) \qquad \mathbf{S}
\begin{pmatrix}
\begin{pmatrix}
\rho \frac{\partial v_x}{\partial t} \\
\rho \frac{\partial v_y}{\partial t} \\
\rho \frac{\partial v_z}{\partial t} \\
\begin{pmatrix}
\frac{\partial \sigma_{xx}}{\partial t} \\
\frac{\partial \sigma_{yy}}{\partial t} \\
\frac{\partial \sigma_{zz}}{\partial t} \\
\frac{\partial \sigma_{xy}}{\partial t} \\
\frac{\partial \sigma_{xz}}{\partial t} \\
\frac{\partial \sigma_{yz}}{\partial t}
\end{pmatrix}
\end{pmatrix}
\end{pmatrix}
=
\begin{pmatrix}
\frac{\partial \sigma_{xx}}{\partial x} + \frac{\partial \sigma_{xy}}{\partial y} + \frac{\partial \sigma_{xz}}{\partial z} \\
\frac{\partial \sigma_{xy}}{\partial x} + \frac{\partial \sigma_{yy}}{\partial y} + \frac{\partial \sigma_{yz}}{\partial z} \\
\frac{\partial \sigma_{xz}}{\partial x} + \frac{\partial \sigma_{yz}}{\partial y} + \frac{\partial \sigma_{zz}}{\partial z} \\
\frac{\partial v_x}{\partial x} \\
\frac{\partial v_y}{\partial y} \\
\frac{\partial v_z}{\partial z} \\
\frac{\partial v_x}{\partial y} + \frac{\partial v_y}{\partial x} \\
\frac{\partial v_x}{\partial z} + \frac{\partial v_z}{\partial x} \\
\frac{\partial v_y}{\partial z} + \frac{\partial v_z}{\partial y}
\end{pmatrix},
$$

where $\mathbf{S} = \mathbf{S}^T > 0$ is the compliance matrix given in Equation (2.3) and $\rho : \Omega \mapsto \mathbb{R}_+$ is the density of the medium. The first three equations in (2.1) describe the conservation of momentum, and the latter six encode time derivative of Hookes law in three space dimensions.

It is convenient to work with Equation (2.1) in its general basis form. Let $\boldsymbol{e} \coloneqq \{\boldsymbol{e}_1, \boldsymbol{e}_2, \boldsymbol{e}_3\}$ be a basis for $\mathbb{R}^3$, then we may recast this PDE system into its conservative and non-conservative components by introducing the anti-symmetric form [7]

$$
(2.2) \qquad \boldsymbol{P}^{-1} \frac{\partial \boldsymbol{Q}}{\partial t} = \nabla \cdot \boldsymbol{F}(\boldsymbol{Q}) + \sum_{\xi \in \{x,y,z\}} \boldsymbol{B}_\xi(\nabla \boldsymbol{Q}),
$$

where $\boldsymbol{Q} \coloneqq (\boldsymbol{v}, \boldsymbol{\sigma})^T$,

$$
(2.3) \qquad \boldsymbol{P} = \begin{pmatrix} \rho^{-1}\mathbf{1} & \mathbf{0} \\ \mathbf{0}^T & \boldsymbol{C} \end{pmatrix}, \qquad \boldsymbol{S}^{-1} \coloneqq \boldsymbol{C} \coloneqq
\begin{pmatrix}
2\mu + \lambda & \lambda & \lambda & 0 & 0 & 0 \\
\lambda & 2\mu + \lambda & \lambda & 0 & 0 & 0 \\
\lambda & \lambda & 2\mu + \lambda & 0 & 0 & 0 \\
0 & 0 & 0 & \mu & 0 & 0 \\
0 & 0 & 0 & 0 & \mu & 0 \\
0 & 0 & 0 & 0 & 0 & \mu
\end{pmatrix},
$$

with $\mu, \lambda \in \mathbb{R}$ are independent Lamé parameters which describe an isotropic medium and

$$
(2.4) \qquad \boldsymbol{F}_\xi(\boldsymbol{Q}) \coloneqq
\begin{pmatrix}
e_{\xi x}\sigma_{xx} + e_{\xi y}\sigma_{xy} + e_{\xi z}\sigma_{xz} \\
e_{\xi x}\sigma_{xy} + e_{\xi y}\sigma_{yy} + e_{\xi z}\sigma_{yz} \\
e_{\xi x}\sigma_{xz} + e_{\xi y}\sigma_{yz} + e_{\xi z}\sigma_{zz} \\
0 \\ 0 \\ 0 \\ 0 \\ 0 \\ 0
\end{pmatrix}, \qquad
\boldsymbol{B}_\xi(\nabla \boldsymbol{Q}) \coloneqq
\begin{pmatrix}
0 \\ 0 \\ 0 \\
e_{\xi x}\frac{\partial v_x}{\partial \xi} \\
e_{\xi y}\frac{\partial v_y}{\partial \xi} \\
e_{\xi z}\frac{\partial v_z}{\partial \xi} \\
e_{\xi y}\frac{\partial v_x}{\partial \xi} + e_{\xi x}\frac{\partial v_y}{\partial \xi} \\
e_{\xi z}\frac{\partial v_x}{\partial \xi} + e_{\xi x}\frac{\partial v_z}{\partial \xi} \\
e_{\xi z}\frac{\partial v_y}{\partial \xi} + e_{\xi y}\frac{\partial v_z}{\partial \xi}
\end{pmatrix},
$$

with $\boldsymbol{F} \coloneqq (\boldsymbol{F}_x, \boldsymbol{F}_y, \boldsymbol{F}_z)^T$ and the basis vectors $\boldsymbol{e}_\xi = (e_{\xi x}, e_{\xi y}, e_{\xi z})^T$. For instance in the standard Cartesian co-ordinate systems we have

$$
(2.5) \qquad \boldsymbol{e}_x = (1,0,0)^T, \qquad \boldsymbol{e}_y = (0,1,0)^T, \qquad \boldsymbol{e}_z = (0,0,1)^T,
$$

which recovers Equation 2.1.

LEMMA 2.1. *Consider the anti-symmetric form given in Equation* (2.2). *For any basis* $\boldsymbol{e}$ *that spans* Ω *we have*

$$\left(\left(\frac{\partial \boldsymbol{Q}}{\partial \xi}\right)^T \boldsymbol{F}_\xi\left(\boldsymbol{Q}\right) - \boldsymbol{Q}^T \boldsymbol{B}_\xi(\nabla \boldsymbol{Q})\right) = 0.$$

Proof. Expanding the matrix multiplication and simplifying yields the result. □

We will find Lemma 2.1 useful in proving stability in our discretisation scheme in complex geometries. It will often be the case that our basis will be defined locally, through finding a set of functions whose partial derivatives evaluated at each point in Ω span $\mathbb{R}^3$. For instance, consider the functions $\text{proj}_\xi : \Omega \mapsto \mathbb{R}$ for $\xi \in \{x, y, z\}$ given through

$$(2.6) \qquad \text{proj}_\xi(x, y, z) := \sum_{\eta \in \{x, y, z\}} \eta \chi_{\{\xi\}}(\eta), \qquad\qquad \chi_B(v) := \begin{cases} 1 & \text{if } v \in B, \\ 0 & \text{otherwise.} \end{cases}$$

These functions form the (local) basis vectors

$$(2.7) \qquad \boldsymbol{e}_\xi|_{(x_0, y_0, z_0)} = \left(\frac{\partial}{\partial x}\text{proj}_\xi, \frac{\partial}{\partial y}\text{proj}_\xi, \frac{\partial}{\partial z}\text{proj}_\xi\right)\Big|_{(x_0, y_0, z_0)},$$

so $\boldsymbol{e}_\xi$ are the contravariant basis defined in (2.5).

2.2. Curvilinear coordinates. Assume $\Omega \subset \mathbb{R}^3$ to be sufficiently smooth such that it can be mapped to the unit cube $\widetilde{\Omega} := [0, 1]^3$. See also Figure 1. If Ω is piece-wise smooth we can partition it into locally smooth sub-blocks and map each sub-block to the unit cube. For simplicity, we will only consider one sub-block here. Let $\Phi : \Omega \mapsto \widetilde{\Omega}$ be a diffeomorphism and adopt the notation

$$\Phi(x, y, z) := (q(x, y, z), r(x, y, z), s(x, y, z)),$$

where $\xi : \Omega \mapsto \mathbb{R}$ for $\xi \in \{q, r, s\}$. Define for $S \subset \Omega$

$$\Phi(S) := \{\Phi(s) \in \widetilde{\Omega} \mid s \in S\}.$$

Assume that $\Phi(\Omega) = \widetilde{\Omega}$, and furthermore the boundary interaction

$$\Phi^{-1}(\{0\} \times [0, 1]^2) = \bigcup_{y, z} \left(\widehat{X}(y, z), y, z\right),$$

for a smooth function $\widehat{X} : \mathbb{R}^2 \mapsto \mathbb{R}$. For example $\widehat{X}(y, z)$ could describe a complex free-surface topography.
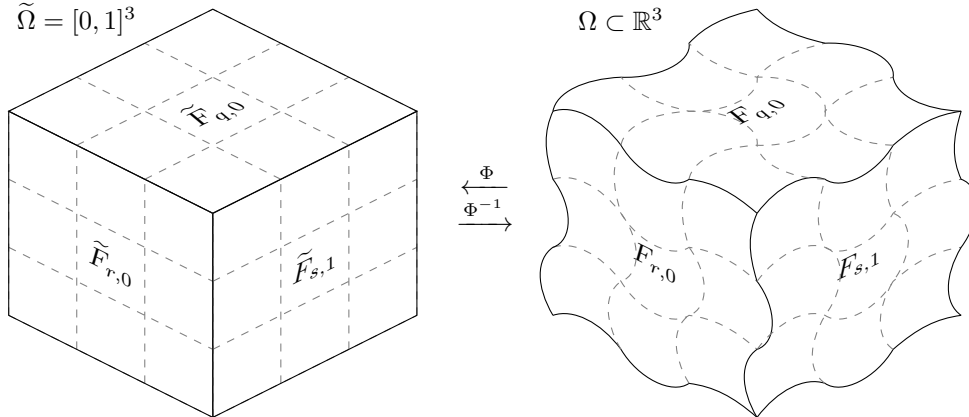

FIG. 1. *Curvilinear coordinate transform and boundary faces of the computational space* $\widetilde{\Omega}$ *and modelling space* Ω.

The Jacobian determinant for Φ^{-1} can be written as

$$J = x_q(y_r z_s - z_r y_s) - y_q(x_r z_s - z_r x_s) + z_q(x_r y_s - y_r x_s).$$

Here ξ_η is the partial derivative $\partial\xi/\partial\eta$ for $\xi, \eta \in \{x, y, z, q, r, s\}$. Similarly,

$$q_x = \frac{1}{J}(y_r z_s - z_r y_s) \qquad r_x = \frac{1}{J}(z_q y_s - y_q z_s) \qquad s_x = \frac{1}{J}(y_q z_r - z_q y_r),$$

$$q_y = \frac{1}{J}(z_r x_s - x_r z_s) \qquad r_y = \frac{1}{J}(x_q z_s - z_q x_s) \qquad s_y = \frac{1}{J}(z_q x_r - x_q z_r),$$

$$q_z = \frac{1}{J}(z_r y_s - y_r x_s) \qquad r_z = \frac{1}{J}(y_q x_s - y_s x_q) \qquad s_z = \frac{1}{J}(x_q y_r - x_r y_q).$$

The spatial derivatives in the transformed coordinates have: the conservative form

$$(2.8) \qquad J\frac{\partial v}{\partial x} = \frac{\partial}{\partial q}(Jq_x v) + \frac{\partial}{\partial r}(Jr_x v) + \frac{\partial}{\partial s}(Js_x v),$$

and the non-conservative form

$$(2.9) \qquad \frac{\partial v}{\partial x} = q_x\frac{\partial v}{\partial q} + r_x\frac{\partial v}{\partial r} + s_x\frac{\partial v}{\partial s}.$$

Although the conservative (2.8) and non-conservative (2.9) transformations of the spatial derivatives are mathematically equivalent, when discretised they give different approximations. Specifically, in the discrete setting, the conservative form (2.8) approximated with an SBP operator preserves the divergence theorem.

For each $(x_0, y_0, z_0) \in \Omega$ and function $\xi \in \{q, r, s\}$ let $\xi_\eta = \frac{\partial\xi}{\partial\eta}$ for $\xi \in \{q, r, s\}$, $\eta \in \{x, y, z\}$, and choose the co-ordinate basis vectors

$$(2.10) \qquad \boldsymbol{e}_\xi = J(\xi_x, \xi_y, \xi_z)\Big|_{(x_0, y_0, z_0)},$$

so Equation (2.1) is transformed to the curvilinear coordinates (q, r, s), with the gradient operator redefined as $\nabla := (\frac{\partial}{\partial q}, \frac{\partial}{\partial r}, \frac{\partial}{\partial s})$, to

$$(2.11) \qquad \widetilde{\boldsymbol{P}}^{-1}\frac{\partial}{\partial t}\boldsymbol{Q} = \nabla \cdot \boldsymbol{F}(\boldsymbol{Q}) + \sum_{\xi \in \{q, r, s\}} \boldsymbol{B}_\xi(\nabla\boldsymbol{Q}),$$

where $\widetilde{\boldsymbol{P}} = J^{-1}\boldsymbol{P}$ and

$$(2.12) \qquad \boldsymbol{F}_\xi(\boldsymbol{Q}) := \begin{pmatrix} J(\xi_x\sigma_{xx} + \xi_y\sigma_{xy} + \xi_z\sigma_{xz}) \\ J(\xi_x\sigma_{xx} + \xi_y\sigma_{xy} + \xi_z\sigma_{xz}) \\ J(\xi_x\sigma_{xx} + \xi_y\sigma_{xy} + \xi_z\sigma_{xz}) \\ 0 \\ 0 \\ 0 \\ 0 \\ 0 \\ 0 \end{pmatrix}, \qquad \boldsymbol{B}_\xi(\nabla\boldsymbol{Q}) \begin{pmatrix} 0 \\ 0 \\ 0 \\ J\xi_x\frac{\partial v_x}{\partial\xi} \\ J\xi_y\frac{\partial v_y}{\partial\xi} \\ J\xi_z\frac{\partial v_z}{\partial\xi} \\ J(\xi_y\frac{\partial v_x}{\partial\xi} + \xi_x\frac{\partial v_y}{\partial\xi}) \\ J(\xi_z\frac{\partial v_x}{\partial\xi} + \xi_x\frac{\partial v_z}{\partial\xi}) \\ J(\xi_z\frac{\partial v_y}{\partial\xi} + \xi_y\frac{\partial v_z}{\partial\xi}) \end{pmatrix}.$$

Note that with the basis vectors $\boldsymbol{e}_\xi = (J\xi_x, J\xi_y, J\xi_z)^T$ we get the anti-symmetric form (2.4).

Remark 2.2. The coordinate transformation in Equation (2.11) is structure preserving, that is Lemma 2.1 holds and we have

$$\left(\left(\frac{\partial \boldsymbol{Q}}{\partial \xi}\right)^T \boldsymbol{F}_\xi(\boldsymbol{Q}) - \boldsymbol{Q}^T \boldsymbol{B}_\xi(\nabla \boldsymbol{Q})\right) = 0,$$

for all $\xi \in \{q, r, s\}$. This will be crucial in deriving high order accurate, structure preserving and provably energy stable scheme for the elastic wave equation in complex geometries.

3. Boundary Conditions. In this section, we formulate linear well-posed boundary conditions in complex geometries. As shown in Figure 1, define the faces of the boundary Γ as

$$F_{\xi,i} := \{(x_0, y_0, z_0) \in \Omega \mid \xi(x_0, y_0, z_0) = i\}$$

for $\xi \in \{q, r, s\}$ and $i \in \{0, 1\}$. Each of the $F_{\xi,i}$ are Lebesgue-almost disjoint and form the boundary of Ω, that is

$$(3.1) \qquad \Gamma = \bigcup_{\xi,i} F_{\xi,i}.$$

Similarly the faces of the computational boundary $\widetilde{\Gamma}$ are given through

$$(3.2) \qquad \widetilde{F}_{\xi,i} := \Phi(F_{\xi,i}) = \{(q, r, s)|_{(x_0,y_0,z_0)} \mid \xi(x_0, y_0, z_0) = i, (x_0, y_0, z_0) \in F_{\xi,i}\},$$

and the boundary $\widetilde{\Gamma}$ of $\widetilde{\Omega}$ is made from the level sets of the functions q, r, s,

$$(3.3) \qquad \widetilde{\Gamma} = \Phi(\Gamma) = \bigcup_{\xi \in \{q,r,s\}} \{(q, r, s)|_{(x_0,y_0,z_0)} \mid \xi(x_0, y_0, z_0) \in \{0, 1\}, (x_0, y_0, z_0) \in \Gamma\}.$$

For a point $(x_0, y_0, z_0) \in F_{\xi,i}$, the unit normal vector to the surface $F_{\xi,i}$ is given by

$$(3.4) \qquad \boldsymbol{n}(x_0, y_0, z_0) = \frac{1}{\sqrt{\xi_x^2 + \xi_y^2 + \xi_z^2}} \begin{pmatrix} \xi_x \\ \xi_y \\ \xi_z \end{pmatrix} \Bigg|_{(x_0,y_0,z_0)},$$

where ξ_x, ξ_y, ξ_z are the partial derivatives of ξ with respect to x, y, z respectively.

For each normal vector $\boldsymbol{n}(x_0, y_0, z_0)$, we can form a locally spanning orthonormal basis with the vectors $\boldsymbol{m}(x_0, y_0, z_0)$ and $\boldsymbol{l}(x_0, y_0, z_0)$ given through a change of variable to the computational space

$$\boldsymbol{m}(x_0, y_0, z_0) := \frac{\boldsymbol{m_0} - \langle \boldsymbol{n}, \boldsymbol{m_0} \rangle \boldsymbol{n}}{|\boldsymbol{m_0} - \langle \boldsymbol{n}, \boldsymbol{m_0} \rangle \boldsymbol{n}|} \Bigg|_{(x_0,y_0,z_0)}, \quad \boldsymbol{l}(x_0, y_0, z_0) := \boldsymbol{n} \times \boldsymbol{m} \Big|_{(x_0,y_0,z_0)},$$

where $\boldsymbol{m_0}$ is a vector not in the span of $\boldsymbol{n}$. For brevity, we often drop the evaluation point when this is clear from context.

Denote the local impedances by Z_η for $\eta \in \{l, m, n\}$, where $Z_n = \rho c_n$ is the p–wave impedance and $Z_m = \rho c_m$, $Z_l = \rho c_l$ are the s–wave impedances. Here, c_n, c_m, c_l are the corresponding effective wave speeds defined We consider specifically an isotropic medium the effective wavespeeds are given by $c_n = c_p$, $c_m = c_l = c_s$.

On the boundary surface, we extract the particle velocity vector and the traction vector, and the local rotation matrix

$$(3.5) \qquad \mathbf{v} = \begin{pmatrix} v_x \\ v_y \\ v_z \end{pmatrix}, \quad \mathbf{T} = \begin{pmatrix} T_x \\ T_y \\ T_z \end{pmatrix} = \begin{pmatrix} \sigma_{xx} & \sigma_{xy} & \sigma_{xz} \\ \sigma_{xy} & \sigma_{yy} & \sigma_{yz} \\ \sigma_{xz} & \sigma_{yz} & \sigma_{zz} \end{pmatrix} \begin{pmatrix} n_x \\ n_y \\ n_z \end{pmatrix}, \quad \mathbf{R} = \begin{pmatrix} \boldsymbol{n}^T \\ \boldsymbol{m}^T \\ \boldsymbol{l}^T \end{pmatrix},$$

where $\det(\mathbf{R}) \neq 0$ and $\mathbf{R}^{-1} = \mathbf{R}^T$.

Next, rotate the particle velocity and traction vectors into the local orthonormal basis, $\mathbf{l}$, $\mathbf{m}$ and $\mathbf{n}$, having

$$(3.6) \qquad v_\eta = (\mathbf{R}\mathbf{v})_\eta, \quad T_\eta = (\mathbf{R}\mathbf{T})_\eta, \quad \eta \in \{l, m, n\}.$$

Plane p–waves and plane s–waves propagating along the normal vector $\mathbf{n}$ on the boundary are given by

$$(3.7) \qquad q_\eta = \frac{1}{2}(Z_\eta v_\eta + T_\eta), \quad p_\eta = \frac{1}{2}(Z_\eta v_\eta - T_\eta), \quad Z_\eta > 0.$$

At the boundary faces $F_{\xi,i}$ defined in (3.2) we consider the linear boundary conditions,

$$(3.8) \qquad \begin{aligned} \frac{Z_\eta}{2}(1 - \gamma_\eta)v_\eta - \frac{1 + \gamma_\eta}{2}T_\eta = 0, \quad (x, y, z) \in F_{\xi,0}, \\ \frac{Z_\eta}{2}(1 - \gamma_\eta)v_\eta + \frac{1 + \gamma_\eta}{2}T_\eta = 0, \quad (x, y, z) \in F_{\xi,1}. \end{aligned}$$

Here γ_η are real parameters with $0 \leq |\gamma_\eta| \leq 1$. The boundary condition (3.8), can describe several physical situations. We have a free-surface boundary condition if $\gamma_\eta = 1$, an absorbing boundary condition if $\gamma_\eta = 0$ and a clamped boundary condition if $\gamma_\eta = -1$. Note that the boundary condition (3.8) satisfy the inequalities

$$(3.9) \qquad \begin{aligned} v_\eta T_\eta > 0, \quad \forall |\gamma_\eta| < 1, \quad \text{and} \quad v_\eta T_\eta = 0, \quad \forall |\gamma_\eta| = 1, \quad \xi \equiv 0, \\ v_\eta T_\eta < 0, \quad \forall |\gamma_\eta| < 1, \quad \text{and} \quad v_\eta T_\eta = 0, \quad \forall |\gamma_\eta| = 1, \quad \xi \equiv 1. \end{aligned}$$

We introduce the boundary terms which are surface integrals encoding the work done by the traction force on the boundary

$$(3.10) \qquad BTs(\boldsymbol{v}, \boldsymbol{T}) := \oint_\Gamma \boldsymbol{v}^T \boldsymbol{T} dS = \sum_{\substack{\xi \in \{q,r,s\} \\ i \in \{0,1\}}} (-1)^{i+1} \int_0^1 \int_0^1 J\sqrt{\xi_x^2 + \xi_y^2 + \xi_z^2}\, \boldsymbol{v}^T \boldsymbol{T} \frac{dqdrds}{d\xi}.$$

LEMMA 3.1. *Consider the well-posed boundary conditions* (3.8) *with* $|\gamma_\eta| \leq 1$. *The boundary term* BTs *defined in* (3.10) *is negative semi-definite,* BTs ≤ 0, *for all* $Z_\eta > 0$.

Proof. Consider the boundary term BTs (v, T) defined in (3.10). With $\mathbf{v}^T \mathbf{T} = (\mathbf{R}\mathbf{v})^T (\mathbf{R}\mathbf{T}) = \sum_{\eta \in \{l,m,n\}} v_\eta T_\eta$, we have

$$\text{BTs}(\boldsymbol{v}, \boldsymbol{T}) = \int_0^1 \int_0^1 \left(\left(J\sqrt{\xi_x^2 + \xi_y^2 + \xi_z^2} \right) \sum_{\eta \in \{l,m,n\}} v_\eta T_\eta \right) \bigg|_{\xi=1} \frac{dqdrds}{d\xi}$$

$$(3.11) \qquad - \sum_{\xi \in \{q,r,s\}} \int_0^1 \int_0^1 \left(\left(J\sqrt{\xi_x^2 + \xi_y^2 + \xi_z^2} \right) \sum_{\eta \in \{l,m,n\}} v_\eta T_\eta \right) \bigg|_{\xi=0} \frac{dqdrds}{d\xi}.$$

Finally, the identity (3.9) completes the proof of the lemma. $\qquad \square$

In the continuous setting, we can show that our PDE has finite energy controlled by the boundary terms, BTs. To begin, for real functions we introduce the L^2 inner product,

$$(3.12) \qquad \langle \mathbf{Q}, \mathbf{F} \rangle := \int_\Omega (\mathbf{Q}^T \mathbf{F})\, dxdydz,$$

and the corresponding energy-norm

$$(3.13) \qquad \|\mathbf{Q}\left(\cdot, \cdot, \cdot, t\right)\|_P^2 = \left\langle \mathbf{Q}, \frac{1}{2}\mathbf{P}^{-1}\mathbf{Q} \right\rangle = \int_\Omega \left(\sum_{\eta \in \{x,y,z\}} \frac{\rho}{2}v_\eta^2 + \frac{1}{2}\boldsymbol{\sigma}^T S \boldsymbol{\sigma} \right) dxdydz.$$

The weighted L^2-norm $\|\mathbf{Q}\left(\cdot, \cdot, \cdot, t\right)\|_P^2$ is the mechanical energy, which is the sum of the kinetic energy and the strain energy.

THEOREM 3.2. *The transformed elastic wave equation* (2.11) *in curvilinear coordinates subject to the boundary conditions* (3.8) *satisfies the energy equation*

$$\frac{d}{dt}\|\mathbf{Q}\left(\cdot, \cdot, \cdot, t\right)\|_P^2 = BTs \leq 0.$$

Proof. Consider

$$(3.14) \qquad \frac{d}{dt}\|\mathbf{Q}\left(\cdot, \cdot, \cdot, t\right)\|_P^2 = \left\langle \boldsymbol{Q}, P^{-1}\frac{\partial}{\partial t}\boldsymbol{Q} \right\rangle = \left\langle \boldsymbol{Q}, \nabla \cdot \boldsymbol{F}(\boldsymbol{Q}) + \sum_{\xi \in \{q,r,s\}} \boldsymbol{B}_\xi(\nabla \boldsymbol{Q}) \right\rangle.$$

Expanding the right hand side and applying integration by parts yields

$$(3.15) \qquad \sum_{\xi \in \{q,r,s\}} \left\langle \boldsymbol{Q}, \frac{\partial}{\partial \xi}\boldsymbol{F}_\xi(\boldsymbol{Q}) \right\rangle + \langle \boldsymbol{Q}, \boldsymbol{B}_\xi(\nabla \boldsymbol{Q}) \rangle = \sum_{\xi \in \{q,r,s\}} \left(\langle \boldsymbol{Q}, \boldsymbol{B}_\xi(\nabla \boldsymbol{Q}) \rangle - \left\langle \frac{\partial}{\partial \xi}\boldsymbol{Q}, \boldsymbol{F}_\xi(\boldsymbol{Q}) \right\rangle \right)$$

$$(3.16) \qquad\qquad\qquad\qquad\qquad + BTs(\boldsymbol{v}, \boldsymbol{T}),$$

which from Lemma 2.1 and 3.1 gives the result. □

In the next section, we will derive a numerical approximation of the transformed elastic wave equation (2.11) in curvilinear coordinates subject to the boundary conditions (3.8). We will approximate spatial derivatives using upwind SBP operators and imposed boundary conditions using penalties. To guarantee numerical stability we will prove numerical results analogous to Theorem 3.2.

4. Discretisation. In this section, stable discrete numerical approximation of the transformed elastic wave equation (2.11) in curvilinear coordinates subject to the boundary conditions (3.8) is derived. We use upwind SBP operators [12] to discretise the spatial derivatives, and keep the time variable continuous. The upwind SBP operators come in pairs, the forward difference operator D_+ and the backward difference operator D_-. Our ultimate goal is to carefully combine this pair of upwind SBP operators to preserve, in the discrete setting, the anti-symmetric property given in Lemma 2.1, and derive a conservative scheme. Boundary conditions are then enforced weakly using penalties in a manner that leads to energy stability.

4.1. Discrete spatial derivative. We will use a reference mesh that is uniform across each of the axes to discretise the reference computational cube $\widetilde{\Omega} = [0, 1]^3$. For each $\xi \in \{q, r, s\}$, consider the uniform discretisation of the unit interval $\xi \in [0, 1]$

$$(4.1) \qquad\qquad \xi_i := i/n_\xi \qquad\qquad i \in \{0, \ldots, n_\xi\},$$

where $n_\xi + 1$ is the number of grid-points on the ξ-axis.

We will use upwind SBP operators introduced in [12] to approximate the spatial derivatives, $\frac{\partial}{\partial \xi}$. By combining the operators D_-, D_+ we can respect the integration by parts formula:

$$(4.2) \qquad\qquad \int_0^1 \frac{\partial}{\partial \xi}(f)g\,d\xi + \int_0^1 f\frac{\partial}{\partial \xi}(g)d\xi = f(1)g(1) - f(0)g(0).$$

This will be critical in deriving a stable and conservative numerical approximation of the elastic wave equation in complex geometries.

For each $\xi \in \{q, r, s\}$ define $H_\xi := \text{diag}\left(h_0^{(\xi)}, \ldots, h_{n_\xi}^{(\xi)}\right)$, with $h_j^{(\xi)} > 0$ for all $j \in \{0, 1, \ldots, n_\xi\}$. We mimic the integration by parts property through finding the dual pairing of linear operators $D_{+\xi}, D_{-\xi} : \mathbb{R}^{n_\xi+1} \mapsto \mathbb{R}^{n_\xi+1}$ so that

$$(4.3) \qquad (D_{+\xi}\boldsymbol{f})^T H_\xi \boldsymbol{g} + \boldsymbol{f}^T H_\xi (D_{-\xi}\boldsymbol{g}) = f(\xi_{n_\xi})g(\xi_{n_\xi}) - f(\xi_0)g(\xi_0),$$

for vectors $\boldsymbol{f} = (f(\xi_0), \ldots, f(\xi_{n_\xi}))^T$, $\boldsymbol{g} = (g(\xi_0), \ldots, g(\xi_{n_\xi}))^T$ sampled from weakly differentiable functions of the ξ variable. Furthermore, the matrix $D_{+\xi} + D_{+\xi}^T$ (or $D_{-\xi} + D_{-\xi}^T$) is negative semi-definite to introduce efficient numerical suppression of unresolved high frequency wave modes, for more details see [12, 3].

We make the discussion more formal.

DEFINITION 4.1. *Let $D_{-\xi}, D_{+\xi} : \mathbb{R}^{n_\xi} \mapsto \mathbb{R}^{n_\xi}$ be linear operators that solve Equation 4.3 for a diagonal weight matrix $H_\xi \in \mathbb{R}^{n_\xi \times n_\xi}$. If the matrix $S_+ := D_{+\xi} + D_{+\xi}^T$ or $S_- := D_{-\xi} + D_{-\xi}^T$ is also negative semi-definite, then the 3-tuple $(H_\xi, D_{-\xi}, D_{+\xi})$ is called an upwind diagonal-norm dual-pair SBP operator.*

We call $(H_\xi, D_{-\xi}, D_{+\xi})$ an upwind diagonal-norm dual-pair SBP operator of order m if the accuracy conditions

$$(4.4) \qquad D_{\eta\xi}(\boldsymbol{\xi}^i) = i\boldsymbol{\xi}^{i-1}$$

are satisfied for all $i \in \{0, \ldots, m\}$ and $\eta \in \{-, +\}$ where $\boldsymbol{\xi}^i := (\xi_0^i, \ldots, \xi_{n_\xi}^i)^T$.

Throughout this study, we will use diagonal diagonal-norm dual-pair SBP operators, and they will be simply referred to as upwind SBP operators.

Similar to traditional SBP operators, upwind SBP operators have higher accuracy in the interior, away from the boundaries. The accuracy of the operators is lowered close to the boundaries where special boundary closures are used. Upwind SBP operators with even order $(2p)$-th accuracy in the interior are closed with p-th order accurate stencils close to boundaries. Upwind SBP operators with odd order $(2p+1)$-th accuracy in the interior are closed with p-th order accurate stencils close to boundaries. These operators can yield $(p+1)$-th global order of accuracy.

The 1D SBP operators can be extended to higher space dimensions using tensor products $\otimes$. Let $f(q, r, s)$ denote a 3D scalar function, and $f_{ijk} := f(q_i, r_j, s_k)$ denote the corresponding 3D grid function. The 3D scalar grid function f_{ijk} is rearranged row-wise as a vector $\boldsymbol{f}$ of length $n_q n_r n_s$. For $\xi \in \{q, r, s\}$ and $\eta \in \{-, +\}$ define:

$$(4.5) \qquad \boldsymbol{D}_{\eta\xi} := \bigotimes_{k \in \{q,r,s\}} (\chi_{k=\xi} D_{\eta k} + \chi_{k \neq \xi} I_{n_k}), \qquad \boldsymbol{H} := \bigotimes_{k \in \{q,r,s\}} H_k,$$

where I_{n_ξ} is the identity matrix of size $n_\xi \times n_\xi$, and we take $\chi_{k=\xi} := \chi_{\{\xi\}}(k)$ and $\chi_{k \neq \xi} := 1 - \chi_{k=\xi}$. So $\boldsymbol{D}_{\xi\eta}$ approximates the partial derivative operator in the ξ direction. An inner product on $\mathbb{R}^{n_q+1} \times \mathbb{R}^{n_r+1} \times \mathbb{R}^{n_s+1}$ is induced by $\boldsymbol{H}$ through

$$(4.6) \qquad \langle \boldsymbol{g}, \boldsymbol{f} \rangle_{\boldsymbol{H}} := \boldsymbol{g}^T \boldsymbol{H} \boldsymbol{f} = \sum_{i=0}^{n_q} \sum_{j=0}^{n_r} \sum_{k=0}^{n_s} f_{ijk} g_{ijk} h_i^{(q)} h_j^{(r)} h_k^{(s)}.$$

Further, we have the multi-dimensional SBP property

$$(4.7) \qquad \sum_{\xi \in \{q,r,s\}} \left(\langle \boldsymbol{D}_{-\xi}(\boldsymbol{f}), \boldsymbol{g} \rangle_{\boldsymbol{H}} + \langle \boldsymbol{f}, \boldsymbol{D}_{+\xi}(\boldsymbol{g}) \rangle_{\boldsymbol{H}} \right) = \sum_{\xi \in \{q,r,s\}} S_\xi (\boldsymbol{f}\boldsymbol{g}),$$

where $S_\xi\left(\boldsymbol{f},\boldsymbol{g}\right)$ in the right hand side is the surface cubature, defined by

$$(4.8) \qquad S_q\left(\boldsymbol{fg}\right) = \sum_{i\in\{0,n_q\}} (-1)^{q_i+1} \sum_{j=0}^{n_r} \sum_{k=0}^{n_s} f_{ijk} g_{ijk} h_j^{(r)} h_k^{(s)},$$

$$(4.9) \qquad S_r\left(\boldsymbol{fg}\right) = \sum_{j\in\{0,n_r\}} (-1)^{r_j+1} \sum_{i=0}^{n_q} \sum_{k=0}^{n_s} f_{ijk} g_{ijk} h_i^{(q)} h_k^{(s)},$$

$$(4.10) \qquad S_s\left(\boldsymbol{fg}\right) = \sum_{k\in\{0,n_s\}} (-1)^{s_k+1} \sum_{i=0}^{n_q} \sum_{j=0}^{n_r} f_{ijk} g_{ijk} h_i^{(q)} h_j^{(r)}.$$

Note that $\xi_0 = 0$ and $\xi_{n_\xi} = 1$, for all $\xi \in \{q, r, s\}$.

4.2. Numerical approximation in space. Consider the transformed elastic wave equation (2.11) in curvilinear coordinates, and approximate the spatial operators using the upwind SBP operators. Note that every 3D scalar grid function is rearranged row-wise as a vector of length $n_q n_r n_s$. Therefore the unknown vector field $\mathbf{Q}$ is a vector of length $9 n_q n_r n_s$.

The semi-discrete approximation reads

$$(4.11) \qquad \widetilde{\mathbf{P}}^{-1} \frac{d}{dt} \mathbf{Q} = \boldsymbol{\nabla}_{D_-} \bullet \mathbf{F}\left(\mathbf{Q}\right) + \sum_{\xi\in\{q,r,s\}} \mathbf{B}_\xi \left(\boldsymbol{\nabla}_{D_+} \mathbf{Q}\right),$$

where the discrete operator $\boldsymbol{\nabla}_{D_\eta} = (\mathbf{D}_{\eta q}, \mathbf{D}_{\eta r}, \mathbf{D}_{\eta s})^T$, with $\eta \in \{+, -\}$, is analogous to the continuous gradient operator $\boldsymbol{\nabla} = (\partial/\partial q, \partial/\partial r, \partial/\partial s)^T$. In $\boldsymbol{\nabla}_{D_\eta}$ we have replaced the continuous derivative operators in $\boldsymbol{\nabla}$ with their discrete counterparts.

Remark 4.2. The backward difference operator D_- is used to approximate the spatial derivative for the conservative flux term, whilst the forward difference operator D_+ is an approximant for the non-conservative product term. This combination of upwind operators and the specific choice of the anti-symmetric form (2.11) is critical to deriving a conservative and energy stable scheme for the elastic wave equation in complex geometries.

Note that we have not imposed boundary conditions yet. Numerical boundary treatment will be discussed in the next subsection.

We will now prove the discrete equivalence of Lemma 2.1.

LEMMA 4.3. *Consider the semi-discrete approximation given in Equation 4.11. We have the discrete anti-symmetric form*

$$\left(\left((I_9 \otimes \boldsymbol{D}_{+\xi}) \boldsymbol{Q} \right)^T \boldsymbol{F}_\xi \left(\boldsymbol{Q}\right) - \boldsymbol{Q}^T \mathbf{B}_\xi \left(\boldsymbol{\nabla}_{D_+} \bar{\mathbf{Q}}\right) \right) = 0.$$

Proof. As before, expanding the matrix multiplication and simplifying yields the result. □

Further, for a 3D scalar field $f_{ijk} = f(x_i, y_j, z_k)$ we also introduce the surface cubature

$$(4.12) \qquad \mathbb{I}_{q_i}\left(\mathbf{f}\right) = \sum_{j=0}^{n_r} \sum_{k=0}^{n_s} \left(J_{ijk} \sqrt{q_{xijk}^2 + q_{yijk}^2 + q_{zijk}^2} f_{ijk} \right) h_j^{(r)} h_k^{(s)},$$

$$(4.13) \qquad \mathbb{I}_{r_j}\left(\mathbf{f}\right) = \sum_{i=0}^{n_q} \sum_{k=0}^{n_s} \left(J_{ijk} \sqrt{r_{xijk}^2 + r_{yijk}^2 + r_{zijk}^2} f_{ijk} \right) h_i^{(q)} h_k^{(s)},$$

$$(4.14) \qquad \mathbb{I}_{s_k}\left(\mathbf{f}\right) = \sum_{i=0}^{n_q} \sum_{j=0}^{n_r} \left(J_{ijk} \sqrt{s_{xijk}^2 + s_{yijk}^2 + s_{zijk}^2} f_{ijk} \right) h_i^{(q)} h_j^{(r)}$$

and

$$(4.15) \qquad \mathbb{I}\left(\mathbf{f}\right) = \sum_{\xi \in \{q,r,s\}} \sum_{i \in \{0, n_\xi\}} (-1)^{\xi_i} \, \mathbb{I}_{\xi_i}\left(\mathbf{f}\right).$$

Therefore we have

$$(4.16) \qquad \mathbb{I}\left(\boldsymbol{v}^T \boldsymbol{T}\right) = \sum_{\xi \in \{q,r,s\}} S_\xi \left(\boldsymbol{J} \sqrt{\boldsymbol{\xi}_x^2 + \boldsymbol{\xi}_y^2 + \boldsymbol{\xi}_z^2}, \boldsymbol{v}^T \boldsymbol{T} \right),$$

where the surface cubature S_ξ is defined in (4.8)–(4.10). Here S_ξ approximates integrals on faces of $\widetilde{\Omega}$, whilst $\mathbb{I}_{\xi_\eta}$ approximates integrals over Ω along the slice ξ_η. Thus the boundary surface term $\mathbb{I}\left(\boldsymbol{v}^T \boldsymbol{T}\right)$ is a numerical approximation of continuous counterpart $BTs\left(\boldsymbol{v}, \boldsymbol{T}\right)$ defined in (3.10).

THEOREM 4.4. *Consider the semi-discrete approximation* (4.11) *of the elastic wave equation. We have*

$$\frac{d}{dt} \|\mathbf{Q}\left(\cdot, \cdot, \cdot, t\right)\|_{HP}^2 = \mathbb{I}\left(\boldsymbol{v}^T \boldsymbol{T}\right),$$

where $\mathbb{I}\left(\boldsymbol{v}^T \boldsymbol{T}\right)$ *is the surface term defined in* (4.16).

Proof. Consider

$$(4.17) \qquad \frac{d}{dt} \|\mathbf{Q}\left(\cdot, \cdot, \cdot, t\right)\|_{HP}^2 = \left\langle \boldsymbol{Q}, P^{-1} \frac{\partial}{\partial t} \boldsymbol{Q} \right\rangle_H = \left\langle \boldsymbol{Q}, \boldsymbol{\nabla}_{D_-} \bullet \mathbf{F}\left(\mathbf{Q}\right) + \sum_{\xi \in \{q,r,s\}} \mathbf{B}_\xi \left(\boldsymbol{\nabla}_{D_+} \mathbf{Q}\right) \right\rangle_H.$$

Expanding the right hand side and applying the multi-dimensional SBP property (4.7) yields

$$\sum_{\xi \in \{q,r,s\}} \left(\left\langle \boldsymbol{Q}, \left(I_9 \otimes \boldsymbol{D}_{-\xi}\right) \boldsymbol{F}_\xi\left(\boldsymbol{Q}\right) \right\rangle_H + \left\langle \boldsymbol{Q}, \mathbf{B}_\xi \left(\boldsymbol{\nabla}_{D_+} \bar{\mathbf{Q}}\right) \right\rangle_H \right)$$
$$= \mathbb{I}\left(\boldsymbol{v}^T \boldsymbol{T}\right) + \sum_{\xi \in \{q,r,s\}} \left(\left\langle \boldsymbol{Q}, \boldsymbol{B}_\xi (\boldsymbol{\nabla}_{D_+} \boldsymbol{Q}) \right\rangle_H - \left\langle \left(I_9 \otimes \boldsymbol{D}_{+\xi}\right) \boldsymbol{Q}, \boldsymbol{F}_\xi(\boldsymbol{Q}) \right\rangle_H \right),$$

which from Lemma 4.3 gives the result. $\qquad\square$

5. Boundary treatment. We will now implement the boundary conditions (3.8) weakly using penalties. The idea is to impose the boundary conditions as Simultaneous Approximating Terms (SAT) in (4.11) with appropriate penalty parameters such that the numerical boundary terms do not permit energy growth. We will choose penalty parameters such that a discrete energy estimate is derived.

The semi-discrete approximation with weak enforcement of boundary conditions is

$$(5.1) \qquad \widetilde{\mathbf{P}}^{-1} \frac{d}{dt} \mathbf{Q} = \boldsymbol{\nabla}_{D_-} \bullet \mathbf{F}\left(\mathbf{Q}\right) + \sum_{\xi \in \{q,r,s\}} \mathbf{B}_\xi \left(\boldsymbol{\nabla}_{D_+} \mathbf{Q}\right) + \sum_{\substack{\xi \in \{q,r,s\} \\ i \in \{0, n_\xi\}}} \mathbf{SAT}_{\xi,i}\left(\mathbf{Q}\right),$$

where $\mathbf{SAT}_{\xi,i}$ are penalty terms added to the discrete equation (4.11) at the boundaries to enforce the boundary conditions (3.8). The SAT penalty terms are not unique, they are designed such that the boundary procedure is consistent and the discrete approximation is energy stable. We will consider first the case of a free-surface boundary condition, and proceed later to the general case.

5.1. SAT term for the free-surface boundary condition. We consider specifically the free-surface boundary condition at all boundary surfaces, $F_{\xi,0}$, $F_{\xi,1}$ for all $\xi \in \{q,r,s\}$. With the

free-surface boundary condition, at $F_{\xi,0}$, $F_{\xi,1}$, the traction vector vanishes $(\boldsymbol{T}_x, \boldsymbol{T}_y, \boldsymbol{T}_z) = 0$. We set the SAT terms

$$(5.2) \qquad \mathbf{SAT}_{\xi,0} = \boldsymbol{H}_\xi^{-1} \mathbf{e}_{0_\xi} \boldsymbol{J} \sqrt{\boldsymbol{\xi}_x^2 + \boldsymbol{\xi}_y^2 + \boldsymbol{\xi}_z^2} \left(\boldsymbol{T}_x, \boldsymbol{T}_y, \boldsymbol{T}_z, \mathbf{0}, \mathbf{0}, \mathbf{0}, \mathbf{0}, \mathbf{0}, \mathbf{0}\right)^T ,$$

$$\mathbf{SAT}_{\xi,n_\xi} = -\boldsymbol{H}_\xi^{-1} \mathbf{e}_{n_\xi} \boldsymbol{J} \sqrt{\boldsymbol{\xi}_x^2 + \boldsymbol{\xi}_y^2 + \boldsymbol{\xi}_z^2} \left(\boldsymbol{T}_x, \boldsymbol{T}_y, \boldsymbol{T}_z, \mathbf{0}, \mathbf{0}, \mathbf{0}, \mathbf{0}, \mathbf{0}, \mathbf{0}\right)^T ,$$

where

$$\boldsymbol{H}_q = \left(I_9 \otimes H_q \otimes I_{n_r} \otimes I_{n_s}\right), \quad \boldsymbol{H}_r = \left(I_9 \otimes I_{n_q} \otimes H_r \otimes I_{n_s}\right),$$
$$\boldsymbol{H}_s = \left(I_9 \otimes I_{n_q} \otimes I_{n_r} \otimes H_s\right),$$

$$\mathbf{e}_{0_q} = (I_9 \otimes e_{0_q} e_{0_q}^T \otimes I_{n_r} \otimes I_{n_s}), \qquad \mathbf{e}_{n_q} = (I_9 \otimes e_{n_q} e_{n_q}^T \otimes I_{n_r} \otimes I_{n_s}),$$
$$\mathbf{e}_{0_r} = (I_9 \otimes I_{n_q} \otimes e_{0_r} e_{0_r}^T \otimes I_{n_s}), \qquad \mathbf{e}_{n_r} = (I_9 \otimes I_{n_q} \otimes e_{n_r} e_{n_r}^T \otimes I_{n_s}),$$
$$\mathbf{e}_{0_s} = (I_9 \otimes I_{n_q} \otimes I_{n_r} \otimes e_{0_s} e_{0_s}^T), \qquad \mathbf{e}_{n_s} = (I_9 \otimes I_{n_q} \otimes I_{n_r} \otimes e_{n_s} e_{n_s}^T),$$

$$e_{0_\xi} = (1, 0, 0, \cdots, 0)^T , \quad e_{n_\xi} = (0, 0, 0, \cdots, 1)^T .$$

Here I_9 and I_{n_ξ} are identity matrices of size 9×9 and $n_\xi \times n_\xi$, respectively, and $\mathbf{e}_{0_\xi}$, $\mathbf{e}_{n_\xi}$ are boundary projection operators.

We state the first main result

THEOREM 5.1. *Consider the semi-discrete approximation* (5.1) *of the elastic wave equation with the SAT terms* $\mathbf{SAT}_{\xi,i}$ *defined in* (5.2). *We have*

$$\frac{d}{dt} \|\mathbf{Q}(\cdot, \cdot, \cdot, t)\|_{HP}^2 = 0.$$

Proof. Consider

$$\frac{d}{dt} \|\mathbf{Q}(\cdot, \cdot, \cdot, t)\|_{HP}^2 = \left\langle \boldsymbol{Q}, P^{-1} \frac{\partial}{\partial t} \boldsymbol{Q} \right\rangle_H = \left\langle \boldsymbol{Q}, \boldsymbol{\nabla}_{D_-} \bullet \mathbf{F}(\mathbf{Q}) + \sum_{\xi \in \{q,r,s\}} \mathbf{B}_\xi \left(\boldsymbol{\nabla}_{D_+} \mathbf{Q}\right) \right\rangle_H$$

$$+ \left\langle \boldsymbol{Q}, \sum_{\substack{\xi \in \{q,r,s\} \\ i \in \{0,1\}}} \mathbf{SAT}_{\xi,i}(\mathbf{Q}) \right\rangle_H .$$

By Theorem 4.4 we have

$$(5.3) \qquad \frac{d}{dt} \|\mathbf{Q}(\cdot, \cdot, \cdot, t)\|_{HP}^2 = \mathbb{I}\left(\boldsymbol{v}^T \boldsymbol{T}\right) + \sum_{\substack{\xi \in \{q,r,s\} \\ i \in \{0,n_\xi\}}} \langle \boldsymbol{Q}, \mathbf{SAT}_{\xi,i}(\mathbf{Q})\rangle_H ,$$

with

$$\sum_{i \in \{0,n_\xi\}} \langle \boldsymbol{Q}, \mathbf{SAT}_{\xi,i} \rangle_H = - \sum_{i \in \{0,n_\xi\}} (-1)^{\xi_i + 1} \mathbb{I}_{\xi_i} \left(\mathbf{v}^T \mathbf{T}\right)$$

where $\xi_0 = 0$ and $\xi_{n_\xi} = 1$. We therefore have

$$\sum_{\substack{\xi \in \{q,r,s\} \\ i \in \{0,n_\xi\}}} \langle \boldsymbol{Q}, \mathbf{SAT}_{\xi,i}(\mathbf{Q})\rangle_H = -\mathbb{I}\left(\boldsymbol{v}^T \boldsymbol{T}\right) ,$$

which completes the proof. □

5.2. SAT terms for general boundary conditions. We will now construct the SAT terms for the general boundary condition (3.8). Similar to the DG framework [6, 17, 7], a weak boundary procedure can be derived by constructing boundary data, $\widehat{v}_\eta, \widehat{T}_\eta$, which are the solution of a Riemann-like problem constrained to satisfy the boundary condition (3.8) exactly. SAT penalty terms are constructed by penalizing data, that is $\widehat{v}_\eta, \widehat{T}_\eta$, against the in-going waves only. The construction of boundary data, $\widehat{v}_\eta, \widehat{T}_\eta$, can be found Appendix A. We also refer the reader to [6, 17] for more detailed discussions.

Introduce the penalty terms

$$(5.4) \qquad G_\eta = \frac{1}{2} Z_\eta \left(v_\eta - \widehat{v}_\eta \right) - \frac{1}{2} \left(T_\eta - \widehat{T}_\eta \right) \Big|_{\xi=0}, \quad \widetilde{G}_\eta := \frac{1}{Z_\eta} G_\eta,$$

$$G_\eta = \frac{1}{2} Z_\eta \left(v_\eta - \widehat{v}_\eta \right) + \frac{1}{2} \left(T_\eta - \widehat{T}_\eta \right) \Big|_{\xi=1}, \quad \widetilde{G}_\eta := \frac{1}{Z_\eta} G_\eta.$$

The penalty terms are computed in the transformed coordinates l, m, n. We will now rotate them to the physical coordinates x, y, z, we have

$$(5.5) \qquad \mathbf{G} := \begin{pmatrix} G_x \\ G_y \\ G_z \end{pmatrix} = \mathbf{R}^T \begin{pmatrix} G_n \\ G_m \\ G_l \end{pmatrix}, \quad \widetilde{\mathbf{G}} := \begin{pmatrix} \widetilde{G}_x \\ \widetilde{G}_y \\ \widetilde{G}_z \end{pmatrix} = \mathbf{R}^T \begin{pmatrix} \widetilde{G}_n \\ \widetilde{G}_m \\ \widetilde{G}_l \end{pmatrix}.$$

Note that

$$\left(\mathbf{v}^T \mathbf{G} - \mathbf{T}^T \widetilde{\mathbf{G}} + \mathbf{v}^T \mathbf{T} \right) \Big|_{\xi=0} = \sum_{\eta \in \{l,m,n\}} \left(v_\eta G_\eta - \frac{1}{Z_\eta} T_\eta G_\eta + v_\eta T_\eta \right) \Big|_{\xi=0}$$

$$= \sum_{\eta \in \{l,m,n\}} \frac{1}{Z_\eta} \left(|G_\eta|^2 + p_\eta^2 \left(v_\eta, T_\eta, Z_\eta \right) - q_\eta^2 \left(\widehat{v}_\eta, \widehat{T}_\eta, Z_\eta \right) \right) \Big|_{\xi=0}$$

$$= \sum_{\eta \in \{l,m,n\}} \left(\frac{1}{Z_\eta} |G_\eta|^2 + \widehat{T}_\eta \widehat{v}_\eta \right) \Big|_{\xi=0},$$

$$(5.6)$$

$$\left(\mathbf{v}^T \mathbf{G} + \mathbf{T}^T \widetilde{\mathbf{G}} - \mathbf{v}^T \mathbf{T} \right) \Big|_{\xi=1} = \sum_{\eta \in \{l,m,n\}} \left(v_\eta G_\eta + \frac{1}{Z_\eta} T_\eta G_\eta - v_\eta T_\eta \right) \Big|_{\xi=1}$$

$$= \sum_{\eta \in \{l,m,n\}} \frac{1}{Z_\eta} \left(|G_\eta|^2 + q_\eta^2 \left(v_\eta, T_\eta, Z_\eta \right) - p_\eta^2 \left(\widehat{v}_\eta, \widehat{T}_\eta, Z_\eta \right) \right) \Big|_{\xi=1}$$

$$= \sum_{\eta \in \{l,m,n\}} \left(\frac{1}{Z_\eta} |G_\eta|^2 - \widehat{T}_\eta \widehat{v}_\eta \right) \Big|_{\xi=1}.$$

We introduce the SAT vector that matches the eigen–structure of the elastic wave equation

$$(5.7) \qquad \mathbf{SAT}_0 = \begin{pmatrix} G_x \\ G_y \\ G_z \\ -n_x \widetilde{G}_x, \\ -n_y \widetilde{G}_y \\ -n_z \widetilde{G}_z, \\ -\left(n_y \widetilde{G}_x + n_x \widetilde{G}_y \right) \\ -\left(n_z \widetilde{G}_x + n_x \widetilde{G}_z \right) \\ -\left(n_z \widetilde{G}_y + n_y \widetilde{G}_z \right) \end{pmatrix}, \quad \mathbf{SAT}_{n_\xi} = \begin{pmatrix} G_x \\ G_y \\ G_z \\ n_x \widetilde{G}_x, \\ n_y \widetilde{G}_y \\ n_z \widetilde{G}_z, \\ \left(n_y \widetilde{G}_x + n_x \widetilde{G}_y \right) \\ \left(n_z \widetilde{G}_x + n_x \widetilde{G}_z \right) \\ \left(n_z \widetilde{G}_y + n_y \widetilde{G}_z \right) \end{pmatrix}.$$

Here, $\mathbf{n} = (n_x, n_y, n_z)^T$ is the unit normal vector on the boundary defined in (3.4). Note that

(5.8) $$\mathbf{Q}^T \mathbf{SAT}_0 = \mathbf{v}^T \mathbf{G} - \mathbf{T}^T \widetilde{\mathbf{G}}, \quad \mathbf{Q}^T \mathbf{SAT}_{n_\xi} = \mathbf{v}^T \mathbf{G} + \mathbf{T}^T \widetilde{\mathbf{G}}.$$

Finally, the SAT terms for the general boundary conditions are defined as follows

(5.9) $$\mathbf{SAT}_{\xi,i} = -\boldsymbol{H}_\xi^{-1} \mathbf{e}_{\xi,i} \boldsymbol{J} \sqrt{\boldsymbol{\xi}_x^2 + \boldsymbol{\xi}_y^2 + \boldsymbol{\xi}_z^2} \mathbf{SAT}_i.$$

Introduce the fluctuation term

(5.10) $$F_{luc}\left(\boldsymbol{G}, \mathbf{Z}\right) := -\sum_{\xi \in \{q,r,s\}} \sum_{i \in \{0,n_\xi\}} \mathbb{I}_{\xi_i} \left(\sum_{\eta=l,m,n} \frac{1}{Z_\eta} |G_\eta|^2 \right) \leq 0,$$

and discrete boundary surface terms $\mathbb{I}\left(\widehat{\mathbf{v}}^T \widehat{\mathbf{T}}\right)$. Note that

(5.11) $$\mathbb{I}\left(\widehat{\mathbf{v}}^T \widehat{\mathbf{T}}\right) = \sum_{\xi \in \{q,r,s\}} S_\xi \left(\boldsymbol{J} \sqrt{\boldsymbol{\xi}_x^2 + \boldsymbol{\xi}_y^2 + \boldsymbol{\xi}_z^2}, \widehat{\mathbf{v}}^T \widehat{\mathbf{T}} \right),$$

where the surface cubature S_ξ is defined in (4.8)–(4.10). Note also that by (A.6) the boundary term is never positive, $\mathbb{I}\left(\widehat{\mathbf{v}}^T \widehat{\mathbf{T}}\right) \leq 0$ for all $|\gamma_\eta| \leq 1$, and by (5.10) the fluctuation term is never positive, $F_{luc}\left(\boldsymbol{G}, \mathbf{Z}\right) \leq 0$. We state the second main result

THEOREM 5.2. *Consider the semi-discrete approximation* (5.1) *of the elastic wave equation with the SAT-terms* $\mathbf{SAT}_{\xi,i}$ *defined in* (5.9). *We have*

$$\frac{d}{dt} \|\mathbf{Q}\left(\cdot, \cdot, \cdot, t\right)\|_{HP}^2 = F_{luc}\left(\boldsymbol{G}, \mathbf{Z}\right) + \mathbb{I}\left(\widehat{\mathbf{v}}^T \widehat{\mathbf{T}}\right) \leq 0.$$

Proof. Consider

$$\frac{d}{dt} \|\mathbf{Q}\left(\cdot, \cdot, \cdot, t\right)\|_{HP}^2 = \left\langle \boldsymbol{Q}, P^{-1} \frac{\partial}{\partial t} \boldsymbol{Q} \right\rangle_H = \left\langle \boldsymbol{Q}, \boldsymbol{\nabla}_{D_-} \bullet \mathbf{F}\left(\mathbf{Q}\right) + \sum_{\xi = q,r,s} \mathbf{B}_\xi \left(\boldsymbol{\nabla}_{D_+} \mathbf{Q} \right) \right\rangle_H$$
$$+ \left\langle \boldsymbol{Q}, \sum_{\substack{\xi \in \{q,r,s\} \\ i \in \{0,1\}}} \mathbf{SAT}_{\xi,i}\left(\mathbf{Q}\right) \right\rangle_H.$$

By Theorem 4.4 we have

(5.12) $$\frac{d}{dt} \|\mathbf{Q}\left(\cdot, \cdot, \cdot, t\right)\|_{HP}^2 = \mathbb{I}\left(\mathbf{v}^T \mathbf{T}\right) + \sum_{\substack{\xi \in \{q,r,s\} \\ i \in \{0,n_\xi\}}} \left\langle \boldsymbol{Q}, \mathbf{SAT}_{\xi,i}\left(\mathbf{Q}\right) \right\rangle_H,$$

with

$$\left\langle \boldsymbol{Q}, \mathbf{SAT}_{\xi,0} \right\rangle_H = -\mathbb{I}_{\xi_0} \left(\mathbf{v}^T \mathbf{G} - \mathbf{T}^T \widetilde{\mathbf{G}} \right), \quad \left\langle \boldsymbol{Q}, \mathbf{SAT}_{\xi,n_\xi} \right\rangle_H = -\mathbb{I}_{\xi_{n_\xi}} \left(\mathbf{v}^T \mathbf{G} + \mathbf{T}^T \widetilde{\mathbf{G}} \right),$$

and

$$\mathbb{I}\left(\mathbf{v}^T \mathbf{T}\right) = \sum_{\substack{\xi \in \{q,r,s\} \\ i \in \{0,1\}}} (-1)^{\xi_i+1} \mathbb{I}_{\xi_i} \left(\mathbf{v}^T \mathbf{T} \right).$$

By using the identity (5.6) we have

$$
\begin{aligned}
\frac{d}{dt}\|\mathbf{Q}\left(\cdot,\cdot,\cdot,t\right)\|_{HP}^2 = \\
- \sum_{\xi\in\{q,r,s\}} \left(\mathbb{I}_{\xi_0}\left(\mathbf{v}^T\mathbf{G} - \mathbf{T}^T\widetilde{\mathbf{G}} + \mathbf{v}^T\mathbf{T}\right) + \mathbb{I}_{\xi_{n_\xi}}\left(\mathbf{v}^T\mathbf{G} + \mathbf{T}^T\widetilde{\mathbf{G}} - \mathbf{v}^T\mathbf{T}\right)\right) \\
= - \sum_{\xi\in\{q,r,s\}} \left(\mathbb{I}_{\xi_0}\left(\sum_{\eta\in\{l,m,n\}}\frac{1}{Z_\eta}|G_\eta|^2 + \widehat{\mathbf{v}}^T\widehat{\mathbf{T}}\right) + \mathbb{I}_{\xi_{n_\xi}}\left(\sum_{\eta\in\{l,m,n\}}\frac{1}{Z_\eta}|G_\eta|^2 - \widehat{\mathbf{v}}^T\widehat{\mathbf{T}}\right)\right) \\
= F_{luc}\left(\boldsymbol{G},\mathbf{Z}\right) + \mathbb{I}\left(\widehat{\mathbf{v}}^T\widehat{\mathbf{T}}\right) \le 0.
\end{aligned}
$$

(5.13)

The proof is complete. □

The fluctuation term $F_{luc}\left(\boldsymbol{G},\mathbf{Z}\right) \le 0$ adds a little numerical dissipation on the boundary. However, in the limit of mesh refinement the fluctuation term vanishes, that is $F_{luc}\left(\boldsymbol{G},\mathbf{Z}\right) \to 0^+$ as $h \to 0^+$, and we have $\mathbb{I}\left(\widehat{\mathbf{v}}^T\widehat{\mathbf{T}}\right) \to BTs\left(\boldsymbol{v},\boldsymbol{T}\right)$. Thus the discrete main results, Theorems (5.1) and (5.2), are completely analogous to the continuous counterpart, Theorem 3.2.

6. Numerical experiments. In this section, we present numerical experiments. The experiments are designed to evaluate accuracy and demonstrate the efficiency of the upwind SBP operators in resolving scattered high frequency waves from complex geometries on marginally resolved meshes. We will use traditional and upwind SBP operators having 6th order accurate interior stencils and 3rd order accurate boundary stencils [4, 12]. These SBP operators have 4th order global accuracy. To verify accuracy, we compute numerical solution of the 3D benchmark problem LOH1 [9, 10], which has a semi-analytic-solution and compare results. We then show the potential of the upwind scheme by simulating a large scale 3D wave propagation problem with complex geometry at different grid resolutions. The upwind scheme provides comparable results on a marginally resolved grid to the traditional SBP operator on a finer grid, thereby improving computational efficiency for 3D numerical seismic wave simulations.

6.1. Layer over a half-space (LOH1). To verify and assess the numerical accuracy of our upwind method, we choose the Layer Over Homogeneous Half-space (LOH1) [2, 9, 10] benchmark problem, a Seismic wave Propagation and Imaging in Complex media (SPICE) validation code. The LOH1 benchmark has a planar free surface and an internal interface between a thin low velocity (soft) upper-layer and high velocity (hard) lower crust. The material properties for the soft upper-layer and hard lower-half-space are

$$
\begin{aligned}
\rho &= 2600\chi_{\{(x_0,y_0,z_0)\ |\ x_0\le 1\}} + 2700\chi_{\{(x_0,y_0,z_0)\ |\ x_0>1\}}, \\
c_p &= 4000\chi_{\{(x_0,y_0,z_0)\ |\ x_0\le 1\}} + 6000\chi_{\{(x_0,y_0,z_0)\ |\ x_0>1\}}, \\
c_s &= 2000\chi_{\{(x_0,y_0,z_0)\ |\ x_0\le 1\}} + 3343\chi_{\{(x_0,y_0,z_0)\ |\ x_0>1\}}.
\end{aligned}
$$

The wave-speeds have units m/s and the density ρ has units kg/m^3. Note that ρ, c_p and c_s are discontinuous in the medium. The benchmark considers homogeneous initial conditions on the solution $\boldsymbol{Q}$ with the double-couple moment tensor point source

$$
\text{(6.1)} \qquad \boldsymbol{f}(x,y,z,t) = \boldsymbol{M}\boldsymbol{\delta}_{(x_p,y_p,z_p)}(x,y,z)g(t), \qquad g(t) := \frac{t}{T^2}\exp(-t/T), \quad T = 0.1 \ \ s,
$$

located 2 km at depth $(x_p,y_p,z_p) = (2,0,0)$, where $\boldsymbol{\delta}$ is the three dimensional Dirac distribution and $\boldsymbol{M} = (0,0,0,0,0,0,0,0,M_0)$ where $M_0 = 10^{18}$ Nm is the moment magnitude. In the z and y directions, the domain of the problem is unbounded. In the positive x direction (in-towards the Earth), the domain is also unbounded with the Earth's surface $x = 0$ having the free surface,

traction-free, boundary condition $(\boldsymbol{T}_x, \boldsymbol{T}_y, \boldsymbol{T}_z) = 0$. To deal with the unbounded domain, we use the PML [5] to absorb outgoing waves and prevent artificial reflections from the bounded computational domain. We take the modelling space to be $\Omega = [0, 6] \times [-5, 15]^2$, two levels of uniform mesh refinements $h = 100$ m and $h = 50$ m across each axis in Ω. To evaluate the results of our schemes, simulated data is compared at the receiver, labelled station 6 and 9 in the LOH1 documentation [2], located on the face $F_{q,0}$ at the locations $(0, 7.348, 7.348)$ and $(0, 8.647, 8.647)$ relative to the epicentre $(0, 0, 0)$.

In Figure 2, it can be seen that both the upwind and traditional schemes have comparable accuracy for the benchmark at 100 m grid resolution. Both of these schemes approximate the analytical solution, with certain peaks in the data containing discrepancies between the numerical and analytical solutions, such as the peak at $\approx 4.3s$ in the V_z data at station 6. Upon refinement to the $h = 50$ m grid resolution in Figure 2, the numerical solutions have converged in most areas of the seismograph. There are some areas of minor disagreements, like the zoomed-in portion of V_z at station 6, where the upwind operator aligns with the analytical solution better than the traditional operator. A similar result is seen in Figure 5 in the appendix. The quantitative envelop misfit and phase misfit [9, 10] for these stations are below %1 for upwind operator and below %2 for the traditional operators.
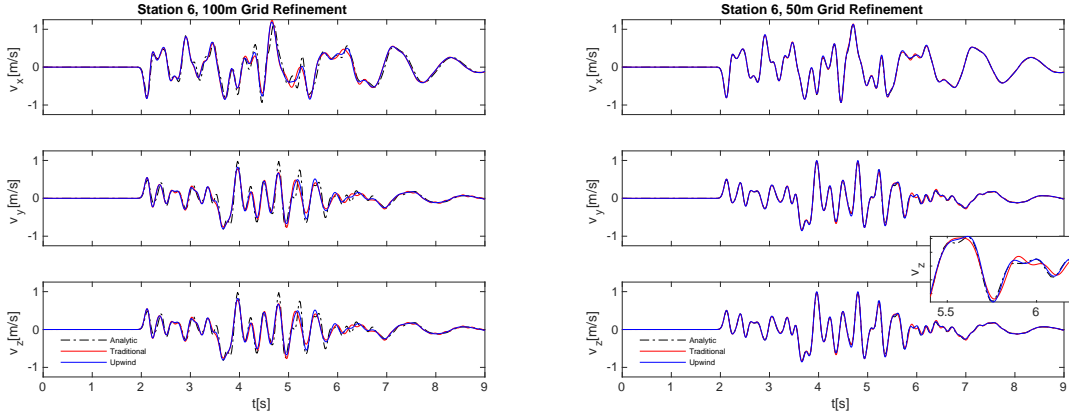

FIG. 2. *Time history of the particle velocity vector at "Station 6" $(x_r, y_r, z_r) = (0, 7.348, 7.348)$ with two levels of uniform mesh refinements $h = 100$ m and $h = 50$ m*

6.2. Zugspitze simulation. We will now present numerical simulations in complex geometries, with a geologically constrained complex non-planar free-surface topography. Zugspitze is the tallest mountain in Germany, lying in the Wetterstein mountain range. The topography of this region is complex, with large variations in altitude across the Earths surface. We extracted the topography data of the Zugspitze region from the high resolution Alpine topography [1]. Accurate and stable simulation of seismic wave propagation in this region is a computationally expensive task, the main reason being the high frequency wave modes generated by scattering from the complex non-planar topography. Numerical simulations using the traditional operators on a resolved grid require about 33000 CPU-hours, including I/O. Our goal is to achieve similar accuracy with less computational resources by utilising upwind SBP operators.

The modelling domain is $\Omega = \bigcup_{y,z \in [-5, 85]} [\widehat{X}(x, y), 80] \times [-5, 85]^2$ with the x-co-ordinate being positive in-towards the Earth, like our previous example, and $\widehat{X}(y, z)$ parameterising the Earth's surface. The material parameter of the region is assumed to be constant and given by $\rho = 2700$ kg/m^3, $c_p = 6000$ m/s and $c_s = 3464$ m/s. The location of the moment tensor point source is at $(10, 10, 10)$. As per the LOH1 experiment, we have free surface boundary conditions at the complex topography $\widehat{X}(y, z)$ and use the PML to prevent artificial reflections from the computational boundaries from

contaminating the solution, that is 10 km at depth. We used 36864 CPU-cores and run the simulation on the $h = 100$ m grid-spacing mesh resolution, with a wall-clock time of ≈ 0.9 hours. On the 200 m grid-spacing mesh resolution, we used 480 CPU-cores with a wall-clock time of ≈ 0.83 hours. In total, the 100 m grid-spacing experiments required about ≈ 33000 CPU-hours, whilst the 200 m grid-spacing only needs ≈ 400 CPU-hours. These CPU-hours also include time and resources needed for I/O, to output the wave fields on the entire topography.

We present the computational results in Figure 4 and Figure 3. Figure 3 shows the snapshots of the numerical solution propagating through time on the surface $\widehat{X}(y, z)$. Here we can see the scattering of high frequency waves conforming to the complex free-surface topography present. In Figure 4 we plot the seismograph for a station placed at $(22.4, 22.4)$ on the Earths surface. We see that upwind operators can resolve high frequency wave modes on a $h = 200$ m mesh resolution without introducing spurious oscillations. The traditional SBP operator resolves some of the important features in the waveform but it also introduces additional large amplitude spurious oscillations which can potentially destroy the accuracy of numerical simulations. Although, the spurious oscillation diminishes with increasing mesh resolutions, that is for $h = 100$ m grid spacing. However, doubling the mesh resolution by using $h = 100$ m grid spacing, increases the computational resources for the 3D problem by several orders of magnitude. Furthermore, the upwind operators suffer less from numerical dispersion errors that are fostered in their traditional operator counterparts. With less computational resources, the upwind operators can potentially resolve high frequency wave modes without introducing poisonous spurious oscillations.
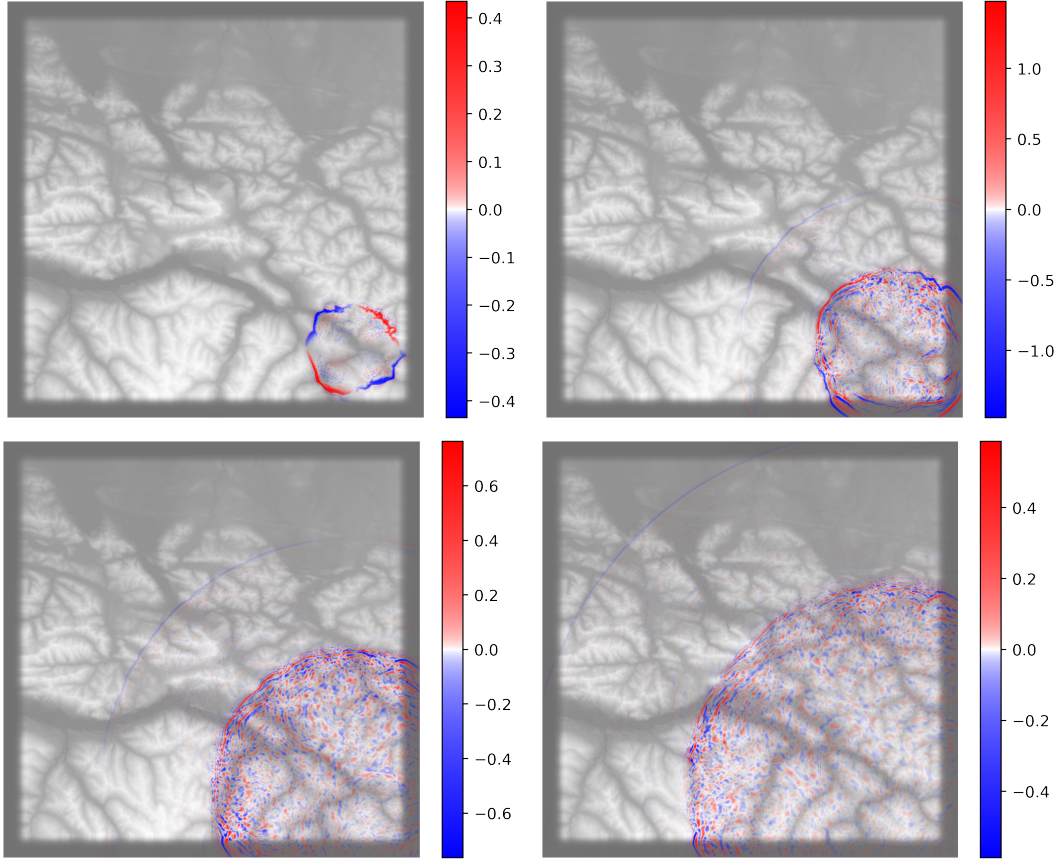

FIG. 3. *Snapshots of upwind SBP simulated wave propagation on $F_{q,0}$ for $t \in \{2.56, 5.95, 9.18, 13\}$ seconds. Here, the background grey represents the altitude given from the underlying topography.*
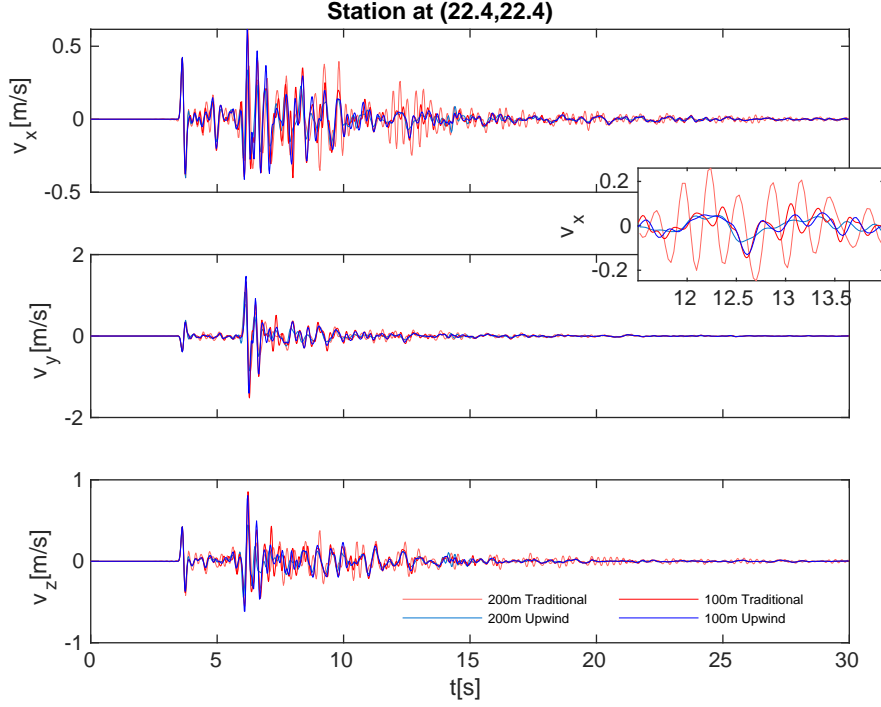
FIG. 4. *Seismograph from a station placed at* $(22.4, 22.4)$ *on the Earths surface.*

7. Conclusion. Upwind SBP finite difference methods are derived and implemented efficiently for the simulation of large-scale elastic wave propagation problems in complex geometries. Using the energy method we show that our implementation is numerically stable. We demonstrate numerically that the method effectively resolves scattered high frequency elastic waves in 3D complex geometries with free surface boundary conditions. When compared to traditional SBP operators based on central finite difference stencils, the upwind counterparts at the same grid resolution are less prone to high-frequency poisonous wave modes. Furthermore, on marginally resolved meshes upwind finite difference schemes have comparable accuracy to traditional SBP operators on finer mesh resolutions. Thus, the upwind SBP operators give a significant gain in computational efficiency for large scale wave propagation problems in 3D-complex geometries.

Our preliminary 3D dynamic earthquake rupture simulations show promise in increasing efficiency through using upwind SBP operators for simulating nonlinear friction laws in elastic solids, and earthquake source modelling.

Appendix A. Hat-variables. The hat-variables encode the solution of the IBVP on the boundary/interface. The hat-variables are constructed such that they preserve the amplitude of the outgoing waves and exactly satisfy the physical boundary conditions [6]. To be more specific, the hat-variables are solutions of the Riemann problem constrained against physical boundary conditions (3.8). We refer the reader to [6, 17] for more detailed discussions. Once the hat-variables are available, we construct physics based numerical flux fluctuations by penalizing data against the incoming characteristics (3.7) at the element faces.

For $Z_\eta > 0$, we define the characteristics

$$(A.1) \qquad q_\eta = \frac{1}{2}\left(Z_\eta v_\eta + T_\eta\right), \quad p_\eta = \frac{1}{2}\left(Z_\eta v_\eta - T_\eta\right), \quad \eta \in \{x, y, z\}.$$

Here, q_η are the left going waves, and p_η are the right going waves. We will construct boundary data which satisfy the physical boundary conditions (3.8) exactly and preserve the amplitude of the outgoing waves q_η at $\xi \equiv 0$, and p_η at $\xi \equiv 1$. That is introduce $\widehat{v}_\eta$ and $\widehat{T}_\eta$ such that

(A.2)
$$q_\eta\left(\widehat{v}_\eta, \widehat{T}_\eta, Z_\eta\right) = q_\eta\left(v_\eta, T_\eta, Z_\eta\right), \quad \text{at} \quad \xi \equiv 0,$$

$$p_\eta\left(\widehat{v}_\eta, \widehat{T}_\eta, Z_\eta\right) = p_\eta\left(v_\eta, T_\eta, Z_\eta\right), \quad \text{at} \quad \xi \equiv 1.$$

The variables $\widehat{v}_\eta$ and $\widehat{T}_\eta$ should also satisfy the physical boundary condition (3.8), and we have

(A.3)
$$\frac{Z_\eta}{2}(1-\gamma_\eta)\widehat{v}_\eta - \frac{1+\gamma_\eta}{2}\widehat{T}_\eta = 0, \quad \text{at} \quad \xi \equiv 0,$$

$$\frac{Z_\eta}{2}(1-\gamma_\eta)\widehat{v}_\eta + \frac{1+\gamma_\eta}{2}\widehat{T}_\eta = 0, \quad \text{at} \quad \xi \equiv 1.$$

The algebraic problem defined by equations (A.2) and (A.3), has a unique solution, namely

(A.4)
$$\widehat{v}_\eta = \frac{(1+\gamma_\eta)}{Z_\eta}q_\eta, \quad \widehat{T}_\eta = (1-\gamma_\eta)q_\eta, \quad \text{at} \quad \xi \equiv 0,$$

$$\widehat{v}_\eta = \frac{(1+\gamma_\eta)}{Z_\eta}p_\eta, \quad \widehat{T}_\eta = -(1-\gamma_\eta)p_\eta, \quad \text{at} \quad \xi \equiv 1.$$

The expressions in (A.4) define a rule to update particle velocity vector and traction vector on the boundaries $\xi = 0, 1$. That is

(A.5)
$$v_\eta = \widehat{v}_\eta, \quad T_\eta = \widehat{T}_\eta, \quad \text{at} \quad \xi \equiv 0, 1.$$

Note in particular that the hat-variables $\widehat{v}_\eta, \widehat{T}_\eta$, satisfy the following inequalities

(A.6)
$$\widehat{T}_\eta \widehat{v}_\eta = \frac{1-\gamma_\eta^2}{Z_\eta}q_\eta^2\left(v_\eta, T_\eta, Z_\eta\right) \geq 0, \quad \text{at} \quad \xi \equiv 0,$$

$$\widehat{T}_\eta \widehat{v}_\eta = -\frac{1-\gamma_\eta^2}{Z_\eta}p_\eta^2\left(v_\eta, T_\eta, Z_\eta\right) \leq 0, \quad \text{at} \quad \xi \equiv 1.$$

The inequalities (A.6) will be crucial in proving numerical stability. Please see also [6] for more details.
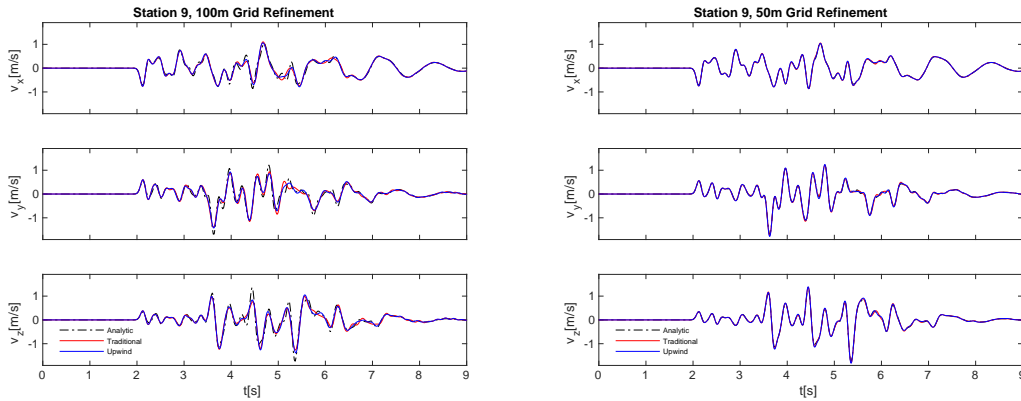
Appendix B. LOH1 Station 9.

FIG. 5. *Time history of the particle velocity vector at "Station 9" $(x_r, y_r, z_r) = (0, 8.647, 8.647)$ with two levels of uniform mesh refinements $h = 100\ m$ and $h = 50\ m$*

REFERENCES

[1] *Copernicus EU-DEM.* https://land.copernicus.eu/pan-european/satellite-derived-products/eu-dem/eu-dem-v1.1, Accessed 2018-03-15.

[2] *Seismowine SPICE.* http://www.sismowine.org/model/WP2_LOH1.pdf.

[3] L. DOVGILOVICH AND I. SOFRONOV, *High-accuracy finite-difference schemes for solving elastodynamic problems in curvilinear coordinates within multi-block approach*, Appl. Numer. Math., 93 (2015), pp. 176–194.

[4] K. DURU AND E. M. DUNHAM, *Dynamic earthquake rupture simulations on nonplanar faults embedded in 3d geometrically complex, heterogeneous elastic solids*, J. Comput. Phys., 305 (2016), pp. 185–207.

[5] K. DURU, J. E. KOZDON, AND G. KREISS, *Boundary conditions and stability of a perfectly matched layer for the elastic wave equation in first order form*, J. Comput. Phys., 303 (2015), pp. 372–395.

[6] K. DURU, L. RANNABAUER, A.-A. GABRIEL, AND H. IGEL, *A new discontinuous galerkin spectral element method for elastic waves with physically motivated numerical fluxes.* https://arxiv.org/abs/1802.06380, 2017.

[7] K. DURU, L. RANNABAUER, A.-A. GABRIEL, O. K. A. LING, H. IGEL, AND M. BADER, *A stable discontinuous galerkin method for linear elastodynamics in geometrically complex media using physics based numerical fluxes.* https://arxiv.org/abs/1907.02658, 2019.

[8] R. GRAVES, T. H. JORDAN, S. CALLAGHAN, E. DEELMAN, E. FIELD, G. JUVE, C. KESSELMAN, P. MAECHLING, G. MEHTA, K. MILNER, D. OKAYA, P. SMALL, AND K. VAHI, *Cybershake: A physics-based seismic hazard model for southern california*, Pure Appl. Geophys., 168 (2011), pp. 367–381.

[9] M. KRISTEKOVÁ, J. KRISTEK, AND P. MOCZO, *Time-frequency misfit and goodness-of-fit criteria for quantitative comparison of time signals*, Geophys. J. Int., 178 (2009), pp. 813–825.

[10] M. KRISTEKOVÁ, J. KRISTEK, P. MOCZO, AND S. M. DAY, *Misfit criteria for quantitative comparison of seismograms*, Bull. Seism. Soc. Am., 96 (2006), pp. 1836–1850.

[11] K. MATTSSON, *Boundary procedures for summation-by-parts operators*, J. Sci. Comput., 18 (2003), pp. 133–153.

[12] K. MATTSSON, *Diagonal-norm upwind sbp operators*, J. Comput. Phys., 335 (2017), pp. 283–310.

[13] S. A. M.H. CARPENTER, D. GOTTLIEB, *Time-stable boundary conditions for finite-difference schemes solving hyperbolic systems: methodology and application to high-order compact schemes*, J. Comput. Phys., 111 (1994), pp. 220–236.

[14] J. NORDSTRÖM AND M. CARPENTER, *High-order finite difference methods, multidimensional linear problems*, J. Comput. Phys., 173 (2001), pp. 149–174.

[15] O. O'REILLY AND N. A. PETERSSON, *Energy conservative sbp discretizations of the acoustic wave equation in covariant form on staggered curvilinear grids*, J. Comput. Phys., 411 (2020), p. 109386.

[16] L. RAYLEIGH, *On waves propagated along the plane surface of an elastic solid*, Proceedings of the London Mathematical Society, s1-17 (1885), pp. 4–11.

[17] A. REINARZ, D. E. CHARRIER, M. BADER, L. BOVARD, M. DUMBSER, F. F. K. DURU, A.-A. GABRIEL, J.-M. GALLARD, S. KÖPPEL, L. KRENZ, L. RANNABAUER, L. REZZOLLA, P. SAMFASS, M. TAVELLI, AND T. WEINZIERL, *Exahype: An engine for parallel dynamically adaptive simulations of wave problems*, Comput. Phys. Comm., (2020), p. 107251.

[18] B. STRAND, *Summation by parts for finite difference approximations for d/dx*, J. Comput. Phys., 110 (1994), pp. 47–67.

[19] M. SVÄRD, *On coordinate transformation for summation-by-parts operators*, J. Sci. Comput., 20 (2004), pp. 29–42.